ISBN: 978-3-95450-231-8 ISSN: 2673-5490 doi: 10.18429/JACoW-IPAC2023-THPL022

VIRTUAL DIAGNOSTICS FOR LONGITUDINAL PHASE SPACE IMAGING

J. S. Lundquist*, S. Werin, F. Curbis, Department of Physics, Lund University, Lund, Sweden

Abstract

For any linear accelerator, a thorough understanding of the Longitudinal Phase Space (LPS) of the beam is a great advantage. At the synchrotron light source MAX IV the two storage rings are injected with electrons using a 3 GeV linear accelerator, which also serves to provide beam for a short pulse facility (SPF). A newly commissioned Transverse Deflecting Cavity (TDC) is used to reconstruct the full LPS in a separate branch in the SPF after the second bunch compressor. This diagnostics performs a destructive measurement to extract the LPS and can not be used simultaneously with the beamline in the other branch of the SPF. In this paper we present a new virtual diagnostics which utilizes machine learning methods to extract the LPS information from other, non-destructive signals in the MAX IV linac. This involves simulations of the linac including the TDC response, as well as the collection of real data from the new TDC, for use in training artificial neural networks to predict the full LPS.

INTRODUCTION

The 3 GeV linear accelerator at MAX IV serves multiple purposes. It is used for initial injection and recurring top-ups for two storage rings, and it also serves a Short Pulse Facility (SPF) at the end of the linac. Since being brought into operation, the linac has remained with minimal longitudinal diagnostics for the beam. For the benefit of the ongoing scientific work at the SPF, and for the general operation of the linac, a Transverse Deflecting Cavity (TDC) has recently been installed in the SPF on a separate line from the beamline used for experiments. This device allows for imaging of the beam's Longitudinal Phase Space (LPS), i.e. its distribution in time and energy [1]. Figure 1 shows a simplified overview of the MAX IV linac and the SPF area with proposed components and beamlines.

Measuring the LPS with a TDC has the drawback of being a destructive measurement as it relies on the beam impinging on a screen. Furthermore, the TDC is housed in a separate beamline from the one used for delivery and the two being used simultaneously is currently not possible. This introduces an application for a Virtual Diagnostic. This system consists of an Artificial Neural Network (ANN) combining different machine learning methods to extract the LPS information from other, non-destructive signals throughout the linac. This paper reports on the current progress towards setting up a virtual diagnostics for LPS predictions using both simulated and measured data.

DATA COLLECTION

Large amounts of varied data is required for setting up a virtual diagnostics as the ANN requires training to map non-destructive measurements to the LPS information of interest. Each dataset must consist of two parts, an input of non-destructive signals and the corresponding output of LPS information. Such datasets have been collected in two different forms for the results presented in this paper: through *elegant* simulations of the MAX IV linac and through measurements of the TDC output during the early commissioning of the new device.

LPS Measurement with TDC

The TDC measurement of the LPS consists of a two-step process. The first one is the transverse deflection: this is performed by a six meter long RF accelerating structure, wherein the fields accelerate the beam transversely. These fields are phased such that the head and tail of the electron beam receive opposite kicks, turning the beam to project the longitudinal distribution onto a transverse dimension, in this case horizontally [1]. In the second step, the beam moves through a dipole and the resulting dispersion projects the energy distribution onto the other transverse dimension. The beam then impinges on a screen allowing for imaging of the resulting LPS.

A dataset for training a virtual diagnostics should include varied situations in the linac for a mapping of distinct beam conditions to specific TDC outputs [3, 4]. To construct such varied situations, phases of the RF in the accelerating structures of the main linac were scanned within a set range. For each setpoint in phase, a TDC image was collected along with non-destructive measurements throughout the linac. After data collection was completed, post processing of the images was done, including background subtraction and slicing of the images into a 200x500 pixel image to isolate the beam.

The main linac phase was scanned in a ± 5 degree range about the nominal setpoint. These phase values were saved along with the positional readings of 36 different BPMs and the readings from two different charge transformers. A total of 120 setpoints were used with resulting datasets saved, with the last 14 removed as the beam began to end up outside the TDC screen. This left 106 images along with their corresponding inputs to be used for training and testing machine learning models.

Simulations of LPS

As the TDC is still in commissioning (at the time of writing), there are limited possibilities for collecting training datasets and the quality of collected data is limited by the current state of the TDC. In order to further develop the virtual diagnostics to eventually be used on a fully functioning TDC, *elegant* simulations [5] have been done, tracking the beam through the whole linac and the TDC at full capacity. In order to construct a large training dataset of different im-

* johan.lundquist@maxiv.lu.se

ISBN: 978-3-95450-231-8 ISSN: 2673-5490 doi: 10.18429/JACoW-IPAC2023-THPL022

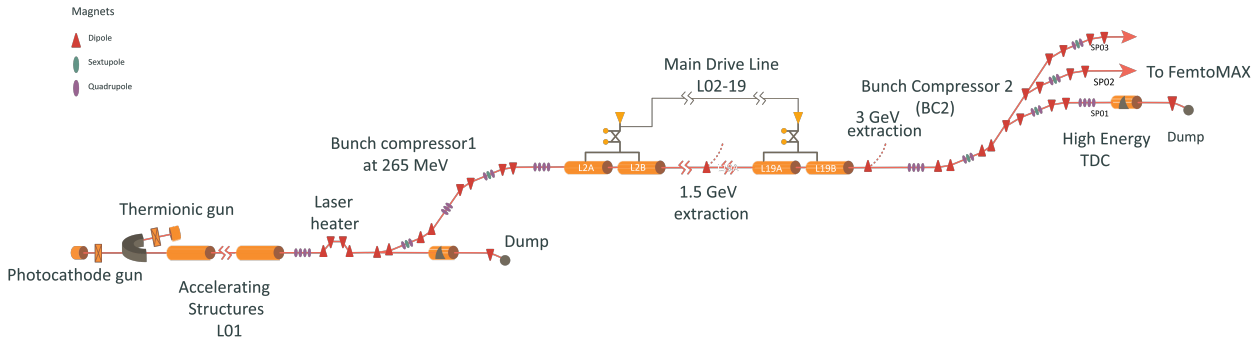

Figure 1: Detailed layout of the MAX IV linac with the currently proposed components of a second TDC and a laser heater, as well as a third beamline for the proposed Soft X-ray FEL [2].

ages and scenarios, parameters have been varied randomly within these simulations.

The RF parameters of two accelerating sections were varied as to construct the dataset of different beam conditions. These sections were an early accelerating structure and the main linac, which is set using a single phase and voltage. Both sections were varied within $\pm 1^\circ$ and $\pm 5\%$ of their nominal phase and voltage. Setpoints outside this range resulted in unrealistic TDC outputs as the *elegant* simulation began to break down. Within this range 2500 randomly selected setpoints were simulated, and along with the setpoints the particle distributions resulting after the TDC process were recorded and later binned into 100x100 pixel images.

Figures-of-Merit

In both the simulated and the measured cases, figures-of-merit (FOM) were also extracted from the stored images. These included the slice energy spread, the full energy spread, the bunch length and the energy chirp. The full energy spread was taken as one σ of a Gaussian fit of the energy profile and the bunch length was taken in the same way for the temporal profile. The slice energy spread was taken as one σ of the Gaussian fit of the energy distribution within a 20 fs window of the simulated distributions and a 60 fs window in the measured data. The energy chirp was taken as the linear tilt of the beam in the images.

VIRTUAL DIAGNOSTICS

The machine learning methods used are commonly known as Multi-Layer Perceptrons (MLPs) and Convolutional Neural Networks (CNNs) [6]. These types of networks have been used to perform two separate predictions in both the simulated and measured case: full image predictions for the output of the TDC on the final screen and predictions of the figures-of-merit.

Image Predictions

The structure of the networks used for the measured and for the simulated cases were in principle very similar. Both were constructed of two densely connected MLP layers of 200 nodes each, followed by a much larger layer with a number of nodes corresponding to the size of the final image, 10000 for the simulated case and 100000 for the measured case. These long vectors were then reshaped into many smaller matrices to be used with the following CNN layers. CNNs consist of matrices of trainable weights that step through the input images to produce the final result. In total, four of these layers were used in the case with measured data and three in the case with simulated data. In both cases, simple mean absolute error was used as the loss function and the ADAM optimizer was used to train the networks [7].

The final performance of the image predictions was scored using R^2 as

$$R^2 = 1 - \frac{\sum (y - \hat{y})^2}{\sum (y - \bar{y})^2}$$

wherein y are the true pixel values in the saved image, $\hat{y}$ are the predicted pixel values and $\bar{y}$ are the mean value of each pixel for the full dataset.

Figures-of-Merit Predictions

The networks used for predicting the four figures-of-merit extracted from each image were much simpler than the larger full image networks. For both measured and simulated data, solely MLP layers were used, in each case two layers of a 100 nodes each, followed by an output layer of four nodes, each corresponding to a figure-of-merit. Here also mean absolute error was used as the loss function and the ADAM optimizer was used to train the networks [7].

RESULTS

In the following subsections the results of four separate networks are shown: both image and figure-of-merit predictions on both measured and simulated data.

Image Predictions

Figure 2 shows three 100x100 images. The center image displays the direct result of the *elegant* simulation after the TDC process, while the image to the left displays the prediction by the neural network. The rightmost image displays the absolute difference between the other two. These images are taken from a test set of 250 images, separated from the

ISBN: 978-3-95450-231-8 ISSN: 2673-5490 doi: 10.18429/JACoW-IPAC2023-THPL022

main dataset before training. On this test dataset, the virtual diagnostic reached a total score of R^2=89.1%.

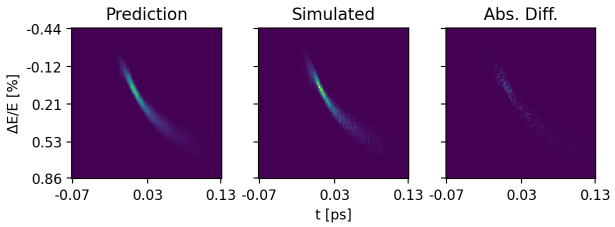

Figure 2: Image prediction of 100x100 pixel simulated TDC image. Leftmost image displays the prediction of the virtual diagnostic, the center image shows the simulated image and the rightmost image shows the absolute difference between the other two.

Figure 3 shows the results on the measured data in a similar structure to Fig. 2. Here also the sum profile is included on each axis of the measured and predicted 200x500 pixel images. Predictions of the measured images reach an R^2 score of 88.1%, but the test dataset consists of only five images. The similarity in performance is promising, though the network can probably handle far less variety in setpoints than the model trained on simulated data as the variety in the training data is much smaller.

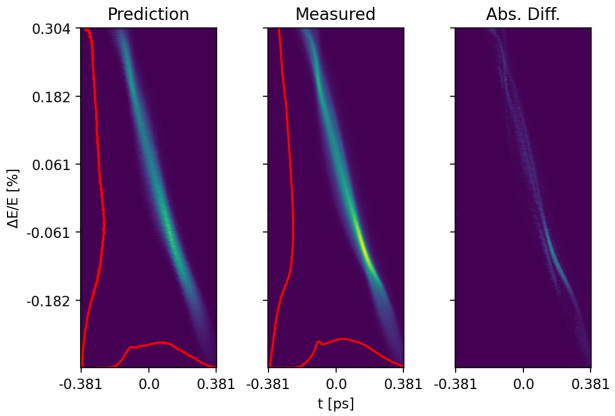

Figure 3: Image prediction of 200x500 pixel measured TDC image. Leftmost image displays the prediction of the virtual diagnostic, the center image shows the measured image and the rightmost image shows the absolute difference between the other two.

Figures-of-Merit Predictions

Figure 4 shows the results of the figure-of-merit predictions using simulated data. From top left to bottom right we see the test data performance on slice energy spread, full energy spread, bunch length and energy chirp. Each plot has the virtual diagnostic's predictions along the vertical axis and the simulated value along the horizontal axis, resulting in the dashed line representing the theoretical perfect predictions. The deviation from this line then shows the errors in the predictions, which are for the most part small. We do see some larger errors in the chirp predictions as the chirp becomes more extreme in some datapoints.

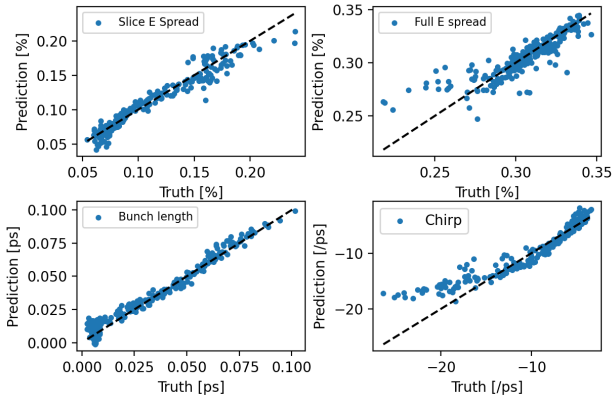

Figure 4: FOM predictions for simulated TDC output. The dashed lines represent ideal predictions.

Figure 5 shows figure-of-merit prediction results on the measured data in a similar structure to Fig. 4. As with the image predictions, here we also have far less data than in the simulated case, being 25 data points isolated for testing.

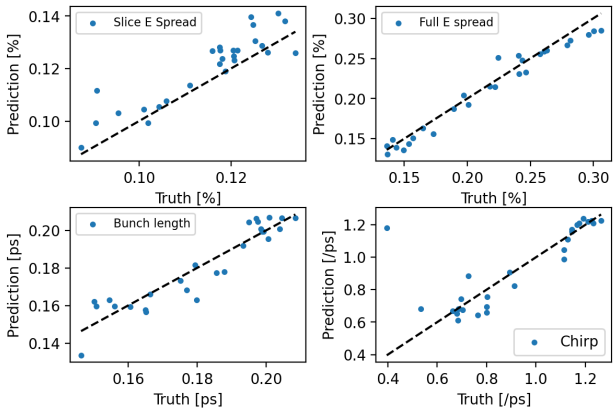

Figure 5: FOM predictions for real TDC output. The dashed lines represent ideal predictions.

OUTLOOK

Virtual diagnostics have been trained and tested on both simulated and measured data from the MAX IV TDC. Predictions using machine learning have been performed of both the full image outputs of the detector, as well as of the figures-of-merit contained within those images. The results on measured data presented here are some of the very first results from the TDC, and future work should focus on larger range scans of linac parameters to create larger and more varied datasets for training and testing future virtual diagnostics.

ISBN: 978-3-95450-231-8 ISSN: 2673-5490 doi: 10.18429/JACoW-IPAC2023-THPL022

REFERENCES

[1] D. Olsson *et al.*, "A Transverse Deflecting Cavity Prototype for the MAX IV LINAC," in *8th International Beam Instrumentation Conference*, 2019, WEPP025. doi:10.18429/JACoW-IBIC2019-WEPP025

[2] W. Qin *et al.*, "The fel in the sxl project at max iv," *Journal of Synchrotron Radiation*, vol. 28, pp. 707–717, 2021. doi:10.1107/S1600577521003465

[3] C. Emma, A. Edelen, M. J. Hogan, B. O'Shea, G. White, and V. Yakimenko, "Machine learning-based longitudinal phase space prediction of particle accelerators," *Phys. Rev. Accel. Beams*, vol. 21, p. 112 802, 11 2018. doi:10.1103/PhysRevAccelBeams.21.112802

[4] C. Emma, A. Edelen, A. Hanuka, B. O'Shea, and A. Scheinker, "Virtual diagnostic suite for electron beam prediction and control at facet-ii," *Information*, vol. 12, p. 61, 2021. doi:10.3390/info12020061

[5] M. Borland, "elegant: A Flexible SDDS-Compliant Code for Accelerator Simulation," in *6th International Computational Accelerator Physics Conference (ICAP 2000)*, 2000. doi:10.2172/761286

[6] I. Goodfellow, Y. Bengio, and A. Courville, *Deep Learning*. MIT Press, 2016, http://www.deeplearningbook.org.

[7] D. P. Kingma and J. Ba, *Adam: A method for stochastic optimization*, 2017.